Chapter 3

Simulations

3.1 PYTHIA

Minimum-bias collisions at $\sqrt{s} = 1.8$ TeV are simulated using PYTHIA version 5.702 and JETSET 7.401 [42, 43]. The combination of PYTHIA and JETSET provide a commonly-used event generator for high-energy collisions of elementary particles based on the parton model [44], and will be hereafter referred to as "PYTHIA". The physics of the collisions that PYTHIA deals with includes

the parton distribution functions of the beam particles, i.e., the flavor of the quarks and the fraction of energy carried by the constituent quarks and gluons of the incident proton and anti-proton,

any radiation from the beam particles, such as the emission of a gluon from a quark, which leads to an initial-state shower,

the hard process between the incoming partons from each shower which produces outgoing particles,

any final-state showers produced by outgoing partons,

the beam remnants, which must return to color-neutral states after losing the interacting partons,

the hadronization of outgoing partons – confinement requires that they form color-neutral hadrons,

and the decay of any unstable outgoing particles.

For the hadronization, PYTHIA uses a string fragmentation model, specifically what is called the Lund model [45]. Its basis is a string connecting a quark and an anti-quark which stretches as the partons move away from each other until it breaks by creating a new quark–anti-quark pair. This continues until only on-mass-shell hadrons remain, where a hadron is a color-singlet pair connected by a small piece of string.

Default values are taken for all parameters except that particles with a mean invariant lifetime $c\tau$ greater than 1 cm are not decayed. This allows the decays of K_s^0 and Λ^0 particles to be studied later.

For non-single diffractive inelastic $p\bar{p}$ collisions at 1.8 TeV, PYTHIA gives mean numbers of particles into the acceptance per event of 0.61 $\pi^{\pm}$'s, 0.15 other charged particles, and 0.70 γ's. The inclusive pseudorapidity distributions, $dN/d\eta$, for charged pions, all charged particles, and photons are shown in Fig. 3.1. (An interesting note is that the larger fraction of particles with $6 < \eta < 10$ in the charged distribution relative to the charged-pion distribution is due to leading protons and anti-protons from double diffractive processes.)

The cross sections for various types of events included in the minimum-bias events generated by PYTHIA are given in Table 3.1. Note that compared to the cross sections reported by CDF (Sec. 2.2), PYTHIA underestimates the total and elastic cross sections, and overestimates the single diffractive.

3.2 GEANT

The particles generated in a collision are then taken as input into a GEANT simulation (GEANT version 3.21 [46]) where they are propagated through the material of the detector. The initial position of the collision primary particles is taken to be $u = v = 0$, and z given by a Gaussian distribution with a mean of 7 in and standard deviation 16.2 in, in order to reproduce the variance of the collision point seen in the data. Cross sections and simulations of processes such as hadronic interactions, electromagnetic processes, ionization by charged particles, multiple scattering, and decays in flight are included in GEANT. Default routines are used for all such processes, as well as the default energies below which particles are not tracked (1 MeV for photons and electrons, 10 MeV for hadrons and muons). The energy deposited in material due to interactions is given at each step, and the secondary particles produced are added to the list of particles to be tracked through the detector.

The energy deposited in the detector elements is used to model the response to particle interactions seen in the real data. At least 4.4(2.2) MeV is required to be deposited in the 1 in (0.5 in)-thick scintillator trigger counters in order to keep the event. Figure 3.2 a shows the energy deposited in the 1 in-thick scintillator counters for minimum bias events, and Fig. 3.3 a shows the energy deposited by single charged pions (minimum-ionizing tracks). In Fig. 3.2 a, the peak for one minimum-ionizing particle passing through the scintillator can be seen around 4.5 MeV, and the smaller peak for two mip's at $9 - 10$ MeV. The first minimum-ionizing peak starts at about 4 MeV, and has a maximum at 4.5 MeV. The low energy background is fairly insignificant. Therefore, any cutoff energy between these values is reasonable. The value 4.4 MeV is chosen to be as large as possible in order to increase the mean number of wires hit in the MWPC's ("NHITS") for triggered events without missing a significant part of the mip peak. (The reason for this will be given in Sec. 3.2.1.)

For the GEANT simulation, the gas in each MWPC is segmented into 128 pieces corresponding to the volume which surrounds each wire in the actual chambers. The wires are not included in the simulation. Plots similar to those for the scintillator energy are given for the chamber pulse heights (energy deposited in a segment) in Fig. 3.2 b and Fig 3.3 b. For single charged pions, the low energy background which falls off around $0.3 - 0.4$ keV where the mip peak begins is presumably due to tracks which pass through more than one segment and deposit some fraction of the minimum-ionizing energy in each segment. For minimum-bias events, the low energy background is much higher and extends into the minimum-ionizing peak. The cutoff value chosen to represent a hit wire is 0.4 keV, where the background falls to a level comparable to the mip contribution. Note that in the actual MWPC's, ionized electrons created by the charged tracks drift to the positively charged wires and the amount of charge collected on a wire determines the pulse height. This may not be linearly related to the energy deposited in the gas; however, direct comparisons of pulse heights in the GEANT and in the data discussed in Sec. 3.2.1 show that this is not an unreasonable assumption.

The energy deposited in each cell of the lead-scintillator electromagnetic calorimeter is recorded, so that it can be used to calibrate the signals from the actual calorimeter.

The other crucial detector element which is included is converter of various thicknesses.

Because of the large observed background of particles due to interactions in material in the forward (detector) region, many objects not related to the detector are included in the simulation. These include the Tevatron beam pipe and abort pipe, the main ring and its abort, support stands, vacuum pumps, the concrete floor, etc. In spite of all these additions, the mean number of wires hit in each MWPC is lower than that in the real data by about a factor of two (see Figs. 3.4, 3.5).

3.2.1 GEANT NHITS study

The NHITS distribution is dependent on the pulse-height and trigger cuts. A lower pulse-height cut allows lower-energy hits to be counted as hits by actual tracks, thus increasing the NHITS in each event. A higher cut on energy deposited in the scintillator counters in order to trigger (i.e. to keep that event) tends to cut out events with less energy or number of tracks going into the detector, so that the mean NHITS of the remaining events is higher than that for all events. The cuts made on the GEANT data are intended to match those in the real data, namely to make cuts based on the signatures of real charged tracks going through the chambers and scintillator. However, we tried varying these cuts through all reasonable (and even unreasonable) values to see if the NHITS distribution of the data could be reproduced by the GEANT simulation. Only 12 of the 24 MWPC's read out pulse-height information, so we use only those chambers in the following analysis. The pulse height is calibrated in terms of charge deposited on the wires, not energy deposited in the gas as it is in GEANT, and is not the same in all chambers. The first step, therefore, is to adjust the energy scales of the chambers in the GEANT so that the mean of a Gaussian fit to the peaks of both the real and GEANT pulse-height distributions are equivalent. The result is shown in Figs. 3.6, 3.7. The mean NHITS in these 12 chambers is 93 for run 867. It is clear in Table 3.2 that there is no combination of pulse-height and scintillator cuts which gives a mean NHITS this high in the GEANT data. For the lowest possible pulse-height cut (pulse height > 0), and the highest shown cut on energy deposited in the scintillator (8 MeV, which practically requires two charged tracks rather than one), the mean NHITS in those 12 chambers is only 79.

The next attempts to find an explanation for the lower NHITS in GEANT include the following:

1. Increasing the thickness of the beampipe from 0.03 in to 0.035 in to check for GEANT problems with the boundary;
2. lowering the energy thresholds of particles for GEANT to track to 1/2 the default value;
3. changing the defaults of GEANT so that delta rays are produced;
4. supposing that the collision point is not where we think it is relative to the pipe, and therefore changing the z of the collision point to 10 in closer to the pipe, or changing x and y by 1 in each towards the pipe.

None of these have much effect on the NHITS. Next we tried adding the main ring and correcting the description of the abort pipe to include the change of material to steel at $z > 275$ in, which increased the mean NHITS by about 20%. Encouraged by this, we added more of the material nearby the detector:

2ft-thick concrete floor, tunnel wall, chamber stands, Tevatron-beampipe and main-ring support stands, and vacuum ion pumps.

The effect on NHITS of material close to the wire chambers was studied in more detail by removing that material. The beampipe is the largest source of non-collision-point tracks hitting the chambers (Fig. 3.8). The abort pipe and the G-10 frames of the wire chambers were also studied (Figs. 3.9, 3.10). The rear chambers are hit by tracks from these sources more than the front; in fact, when all three of the sources are removed, the mean number of hits per event in each chamber is approximately a constant between 3.5 and 4 (Fig. 3.11), as opposed to the roughly linear increase in hits going from about 4 in the front chamber to more than 8 in the last, as in Fig. 3.4. (This is, of course, for lead-out runs. For lead-in runs, the number of hits in the chambers behind the lead is much greater than that in the front due to conversions of primary photons.) In the real data, the number of hits per chamber increases faster than linearly towards the rear of the detector. The addition of the beampipe supports in the GEANT simulation reproduces this effect fairly well. These observations are what led to the compression of the wire chambers which moved them closer to the collision point before the production running.

It has been noted [47] that the multiplicity distributions of low-p_T charged particles in PYTHIA were incorrectly extrapolated from collider data at high p_T. Since the MiniMax detector is more sensitive than conventional collider detectors to low-p_T particles, these can potentially contribute significantly to the NHITS. We tried using HERWIG, another commonly-used event generator (especially for jet studies) to see if the NHITS distribution might be better reproduced. Comparisons of $dN/d\eta$ from non-diffractive PYTHIA events and HERWIG events show that the mean number of particles produced is higher for PYTHIA (see Fig. 3.12 for $dN_{ch}/d\eta$). The NHITS distribution obtained using HERWIG was not significantly different.

Another attempt to increase the mean NHITS in the simulations was to change the defaults for multiple interactions in PYTHIA. The occurrence of hard interactions of more than one parton pair in a hadronic collision is not well understood, and PYTHIA provides several models. The default is that the probability of multiple interactions is equal for all events, with a sharp $p_{\perp min}$ cut-off. It was suggested to us that the option with "multiple interactions assuming a varying impact parameter and a hadronic matter overlap consistent with a double Gaussian matter distribution ... with a continuous turn-off of the cross section at $p_{\perp 0}$" (Ref. [43], p. 222) would give larger multiplicity fluctuations, and therefore possibly larger mean NHITS. The effect of using this model is also negligible.

A study was done by the ALICE Collaboration on MWPC's which are intended to be used in a muon spectrometer at the LHC [48]. The chambers are remarkably similar to the ones used by MiniMax, and therefore the results obtained in the study may be relevant to the performance of the MiniMax chambers. A pion beam was aimed at a lead absorber, and background particles from interactions in the lead were detected in a wire chamber located at the position which was predicted by simulations as the location of the shower maximum. A GEANT simulation proved to underestimate the measured number of charged particles into the chamber by a factor of 2-4. A simulation using stand-alone FLUKA (as opposed to the option of using FLUKA subroutines inside GEANT) produced a distribution of particles much closer to what was actually seen. Further analysis suggested that a significant contribution to the hits in the chambers was due to neutrons interacting in the mylar face of the chamber and knocking out protons which were then detected. Such interactions of low-energy neutrons are included in the stand-alone FLUKA. We have not been able to obtain the stand-alone FLUKA simulation code.

3.2.2 GEANT trigger rates

The trigger rates and cross sections for events in the GEANT simulation from the minimum-bias PYTHIA input are shown in Table 3.1. The total fraction of events which pass the trigger in GEANT is slightly more than 50%, and is higher for lead-in runs than for lead-out by about 1% for all types of events. Single diffractive events in which the proton is dissociated are triggered on about 15% of the time, and about 10% of those with a fragmenting anti-proton pass the trigger. For double diffraction, the fraction is about 20%.

Note that if we add the fraction of triggered single diffractive events (26%) times the single diffractive cross section from CDF (9.46 mb) to the non-single diffractive fraction (79%) times the corresponding CDF cross section (50.87 mb), the result is that we should trigger on 42.7 mb, which agrees very well with the estimate in Sec. 2.2.3.

3.3 DCC generator

The operational definition of DCC used by the MiniMax collaboration is that DCC is a cluster of pions (domain) with neutral fraction f given by the $1/(2\sqrt{f})$ distribution and with near-identical momenta which is non-relativistic in the DCC rest frame. For the studies presented here, the domain size is taken to be on the order of the detector acceptance, and the momentum is such that the DCC is aimed at the center of the acceptance with a reasonably large p_T in the lab frame.

We assume that the pions are non-relativistic in the cm frame of the DCC domain (and therefore refer to the domain as a "snowball"). We take the momentum distribution to be Gaussian with mean $\langle\vec{p}\rangle = 0$ and variance $\langle\vec{p}\cdot\vec{p}\rangle = 3\sigma_p^2$. Since the DCC domain must be large enough to contain physical pions, i.e. have dimensions on the order of a few fm, uncertainty principle arguments require a small momentum, $\sigma_p \sim 50 - 100$ MeV. We use the value $\sigma_p = 100$ MeV, which gives the pions a relatively large momentum in the lab frame, making them easier to detect. If the pions are not too relativistic in the cm frame, then the boosted DCC domain is approximately a circular disk of radius in lego space $R_{DCC} \sim \sigma_p/p_T$. For the MiniMax detector, with acceptance approximately a circle with radius 0.6, a domain with $R_{DCC} \sim 0.7 - 1.0$ would be easiest to find, which implies $p_T = 140\,\mathrm{MeV}$. This size seems reasonable since the typical radius of a jet is 0.7.

We also assume that the number of pions in the DCC domain is approximately independent of the pseudorapidity of the center of the boosted domain. A result of this is that the ratio ψ of the mean energy density of a DCC pion to that of a generically-produced pion is approximately constant. Then the mean number of pions is given by

$$\langle N_\pi \rangle \sim \psi \frac{p_T^{gen}}{p_T} \left(\frac{d^2N}{d\eta d\phi} \right)_{gen} \delta\eta\, \delta\phi,$$

or, substituting in the geometric values,

$$\langle N_\pi \rangle \sim \psi \frac{p_T^{gen}}{p_T} \frac{1}{2\pi} \left(\frac{dN}{d\eta} \right)_{gen} \pi R_{DCC}^2.$$

We take $(dN/d\eta)_{gen} = 6$ in the region of the acceptance, $p_T^{gen} = 500$ MeV, and $\psi = 1$, which gives a mean number of pions $\langle N_\pi \rangle = 5.0$. For a given event, the number of pions is taken from a Poisson distribution about this mean.

Next the charge of the pions is determined according to the $1/(2\sqrt{f})$

distribution. The neutral fraction in a given event is generated using the transformation method, where, if x is a uniform deviate, then $f = x^2$ is distributed according to $1/(2\sqrt{f})$. A uniform deviate y_i is then generated for each of the pions ($i = 1, N_\pi$); if $y_i < f$, the pion is defined to be neutral, otherwise it is defined to be charged.

Figures 3.13-3.15 show for the DCC pions: the momentum distributions, the distributions in η and ϕ for a domain aimed at $\eta = 4.1$ and $\phi = 0.75$, the neutral-fraction distribution and the number distribution. Histograms of the number of events with given numbers of charged and neutral pions, for both total numbers and the numbers of those that enter the acceptance are shown in Fig. 3.16, and can be compared with that from generically-produced pions from PYTHIA in Fig. 3.17.

Unless noted otherwise, all further mention of the DCC generator refers to the use of the parameters given here.

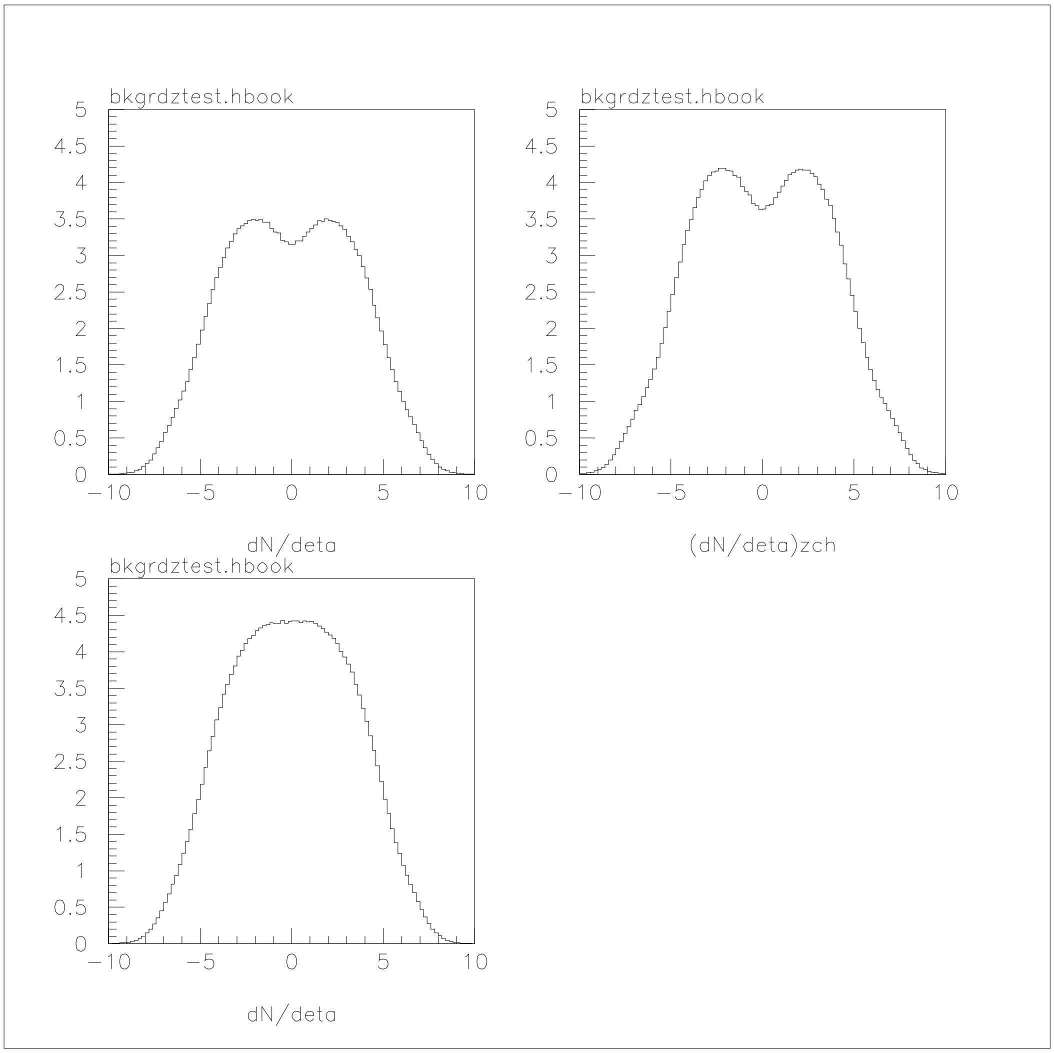

Figure 3.1: Pseudorapidity distribution $dN/d\eta$ for charged pions, all charged particles, and photons.

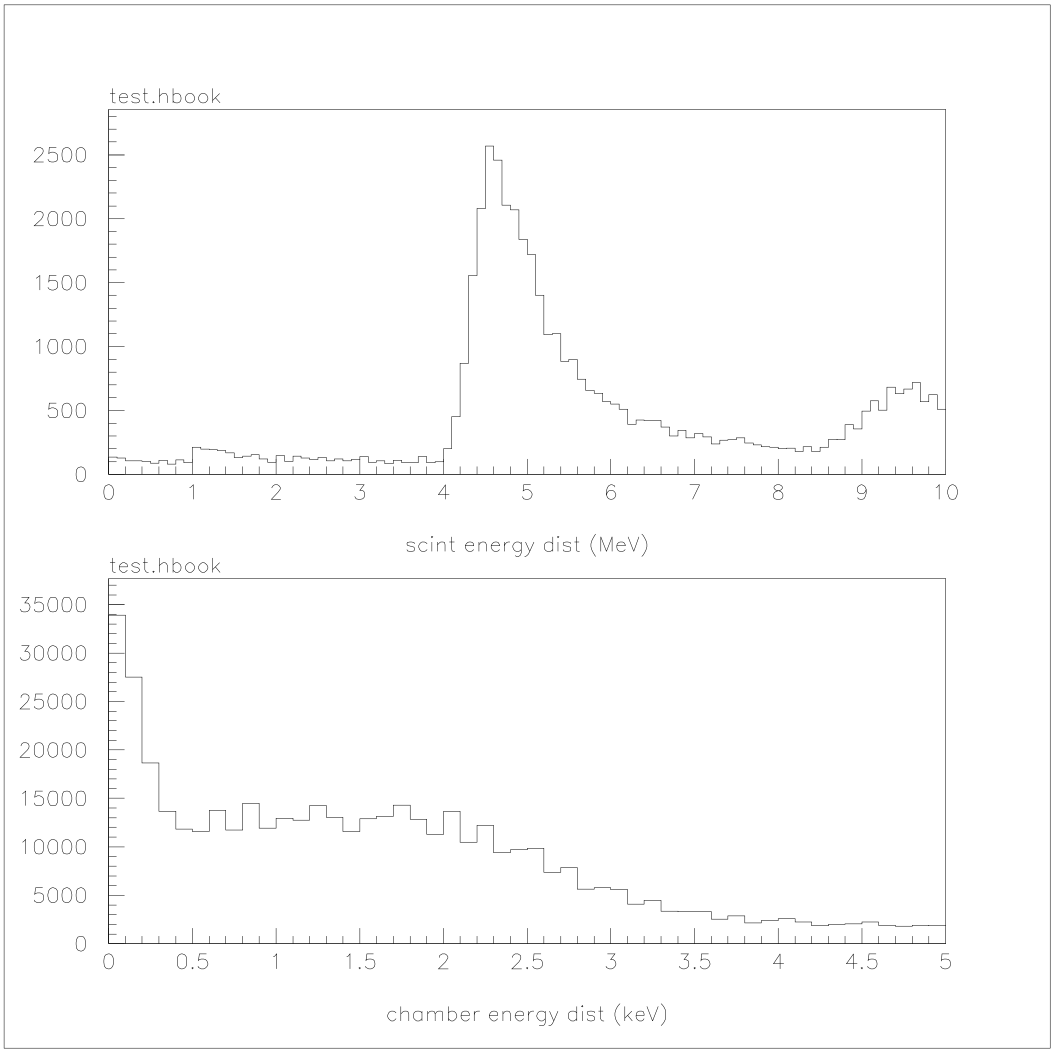

Figure 3.2: Energy deposited in (a) scintillator and (b) chambers in minimum bias events.

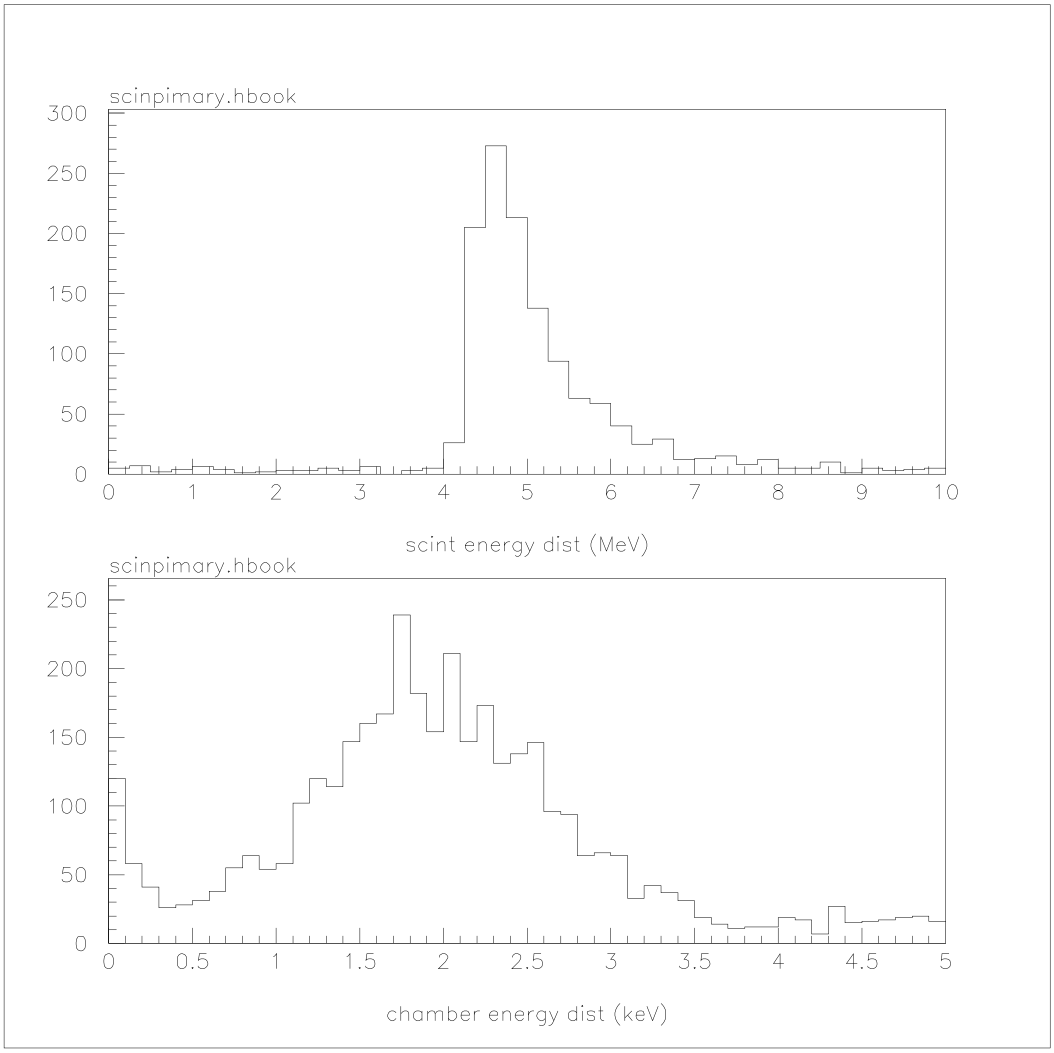

Figure 3.3: Energy deposited in (a) scintillator and (b) chambers by single charged pions.

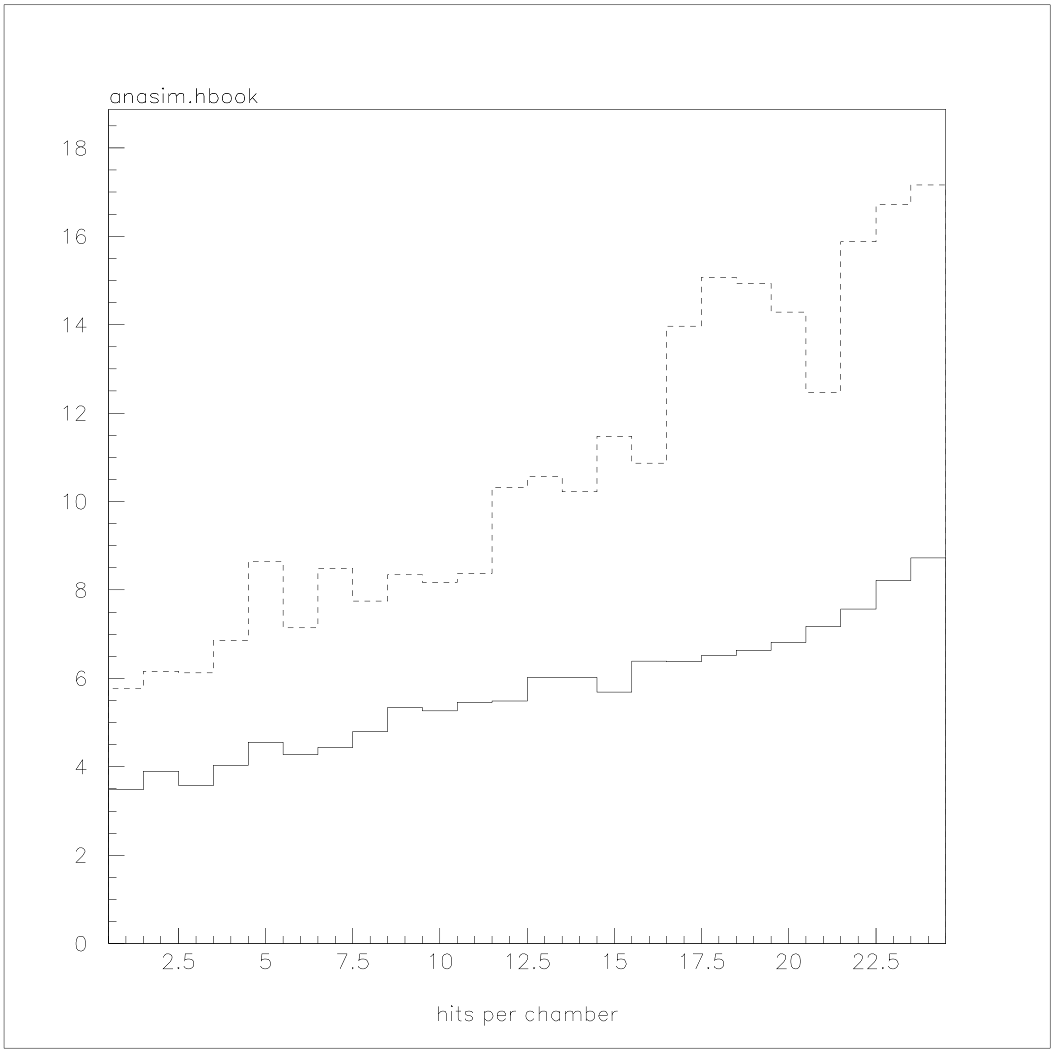

Figure 3.4: Mean number of wire hits per chamber: real (dashed) and GEANT with beam supports, etc (solid).

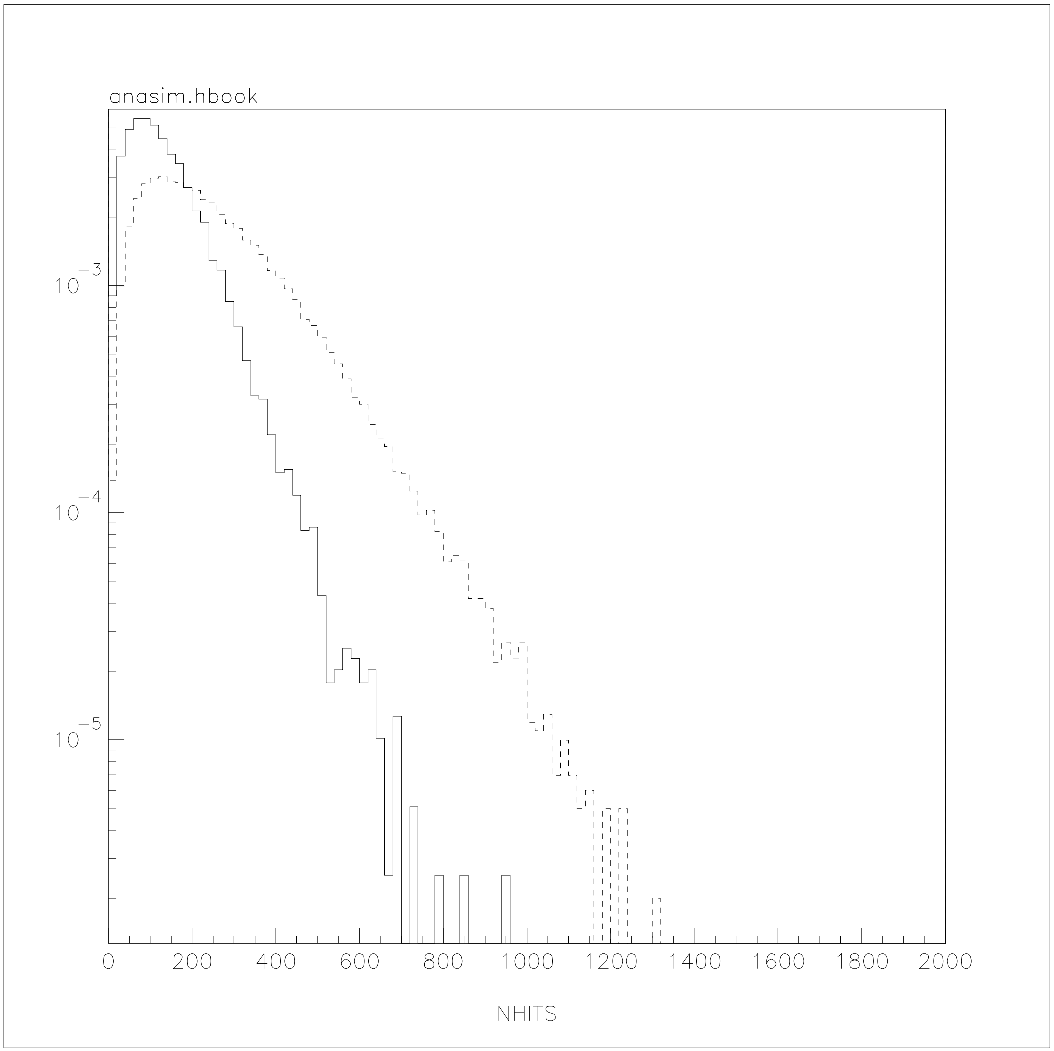

Figure 3.5: Distribution of NHITS: real (dashed) and GEANT with beam supports, etc (solid).

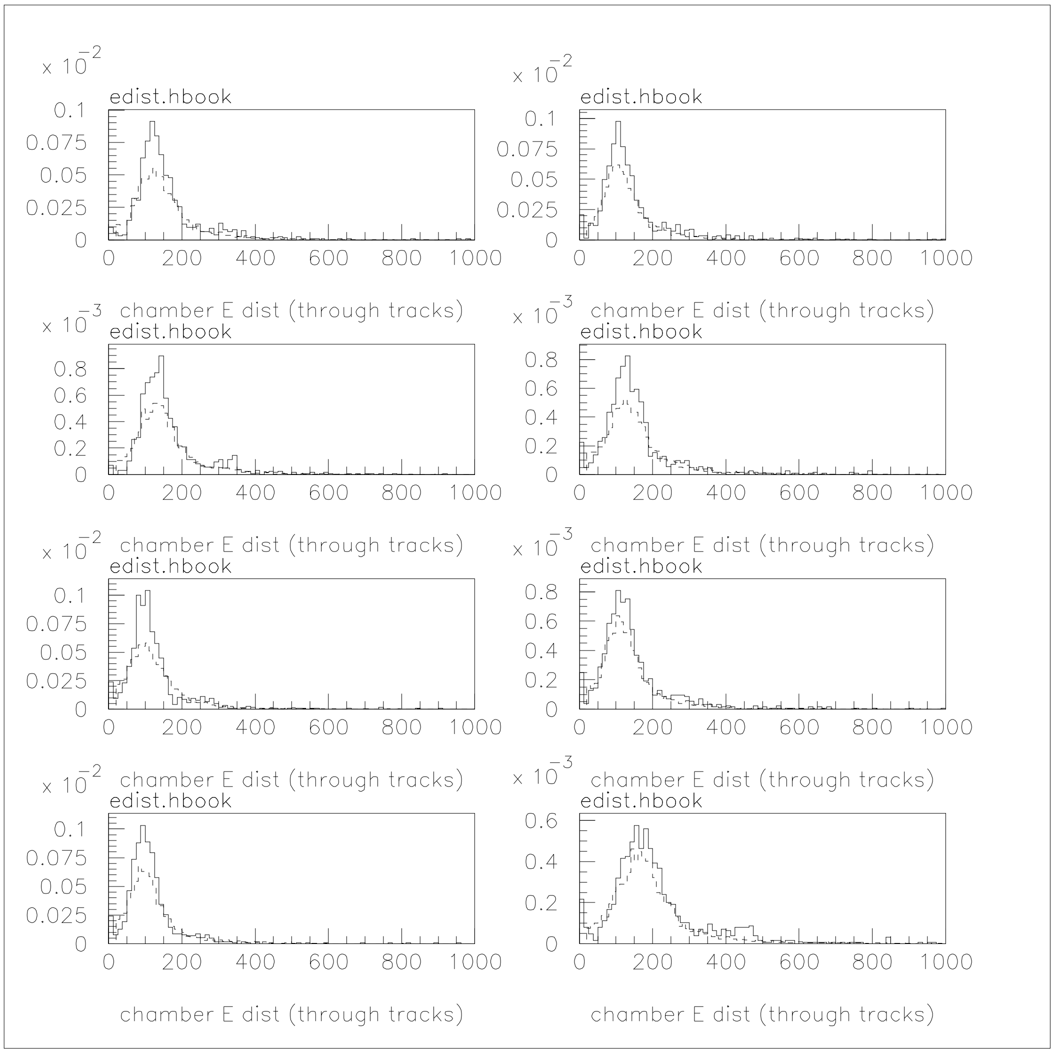

Figure 3.6: Pulse height distributions for chambers 1-4, 9-12, real (dashed) and GEANT (solid).

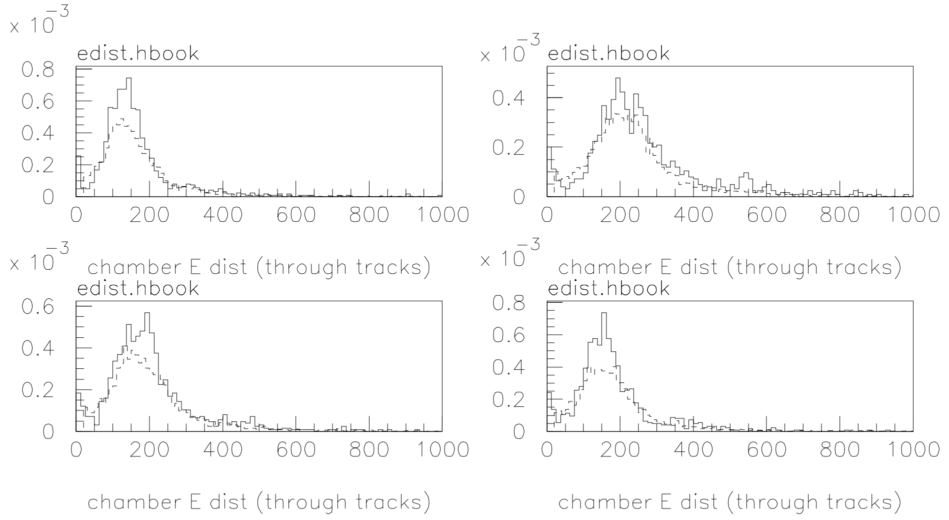

Figure 3.7: Pulse height distributions for chambers 21-24: real (dashed) and GEANT (solid).

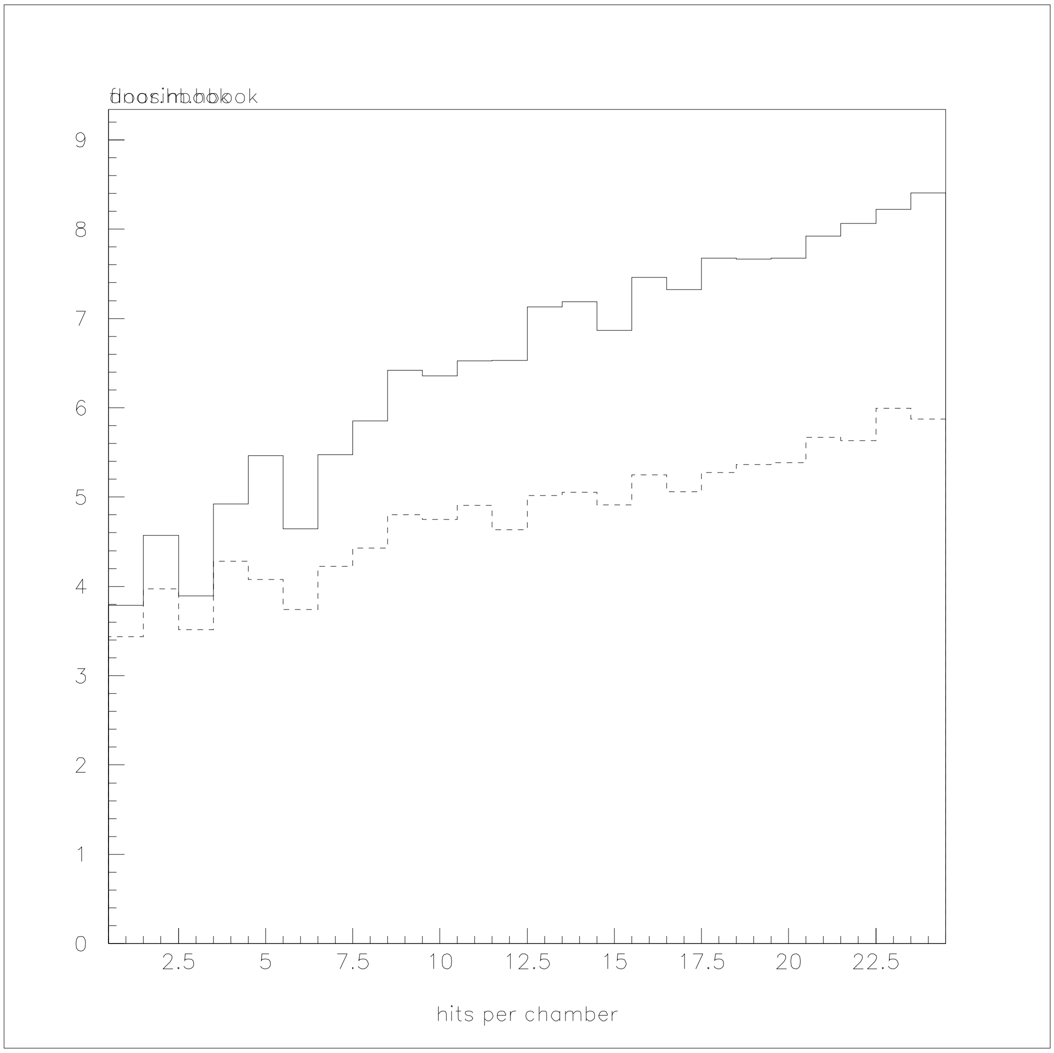

Figure 3.8: Mean number of wire hits in each chamber (solid) and with the beampipe removed (dashed).

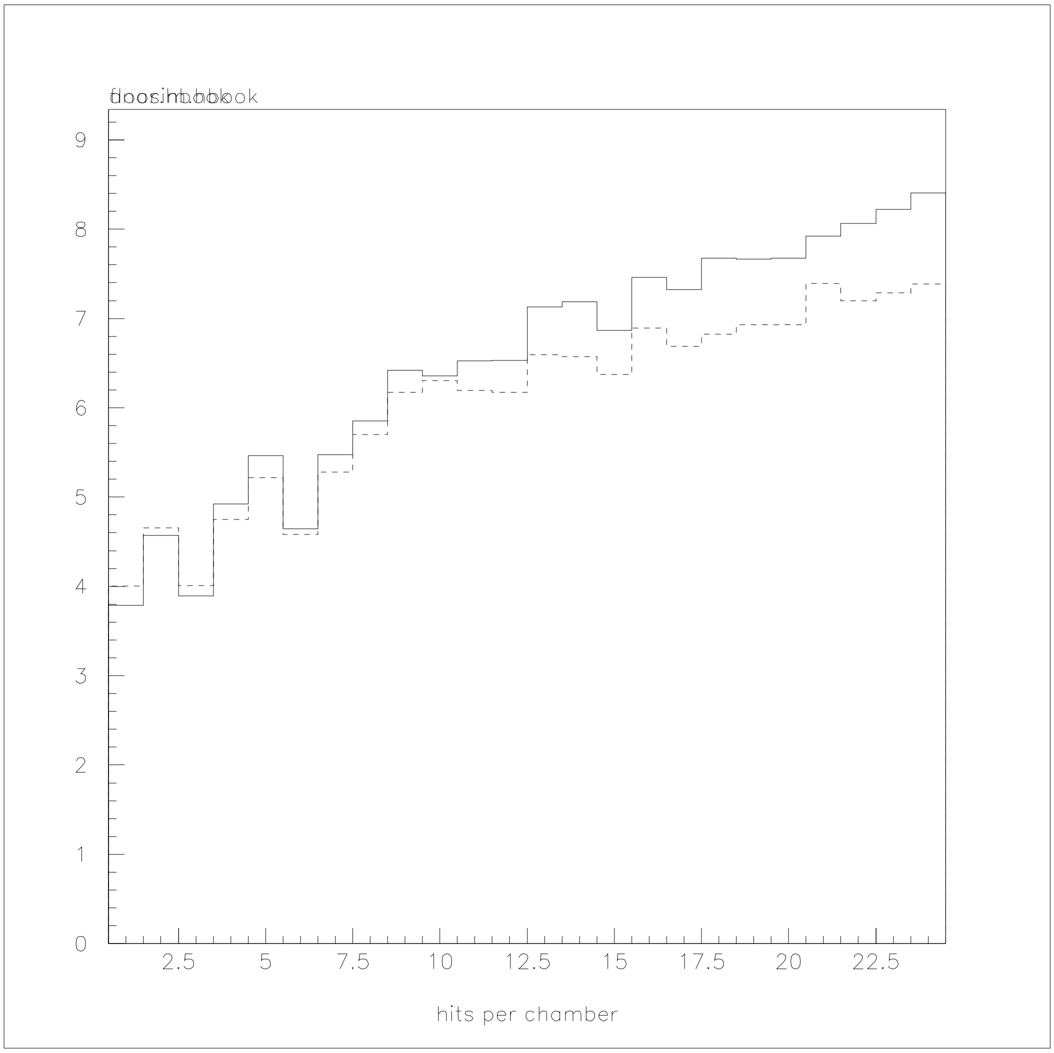

Figure 3.9: Mean number of wire hits in each chamber (solid) and with the abort pipe removed (dashed).

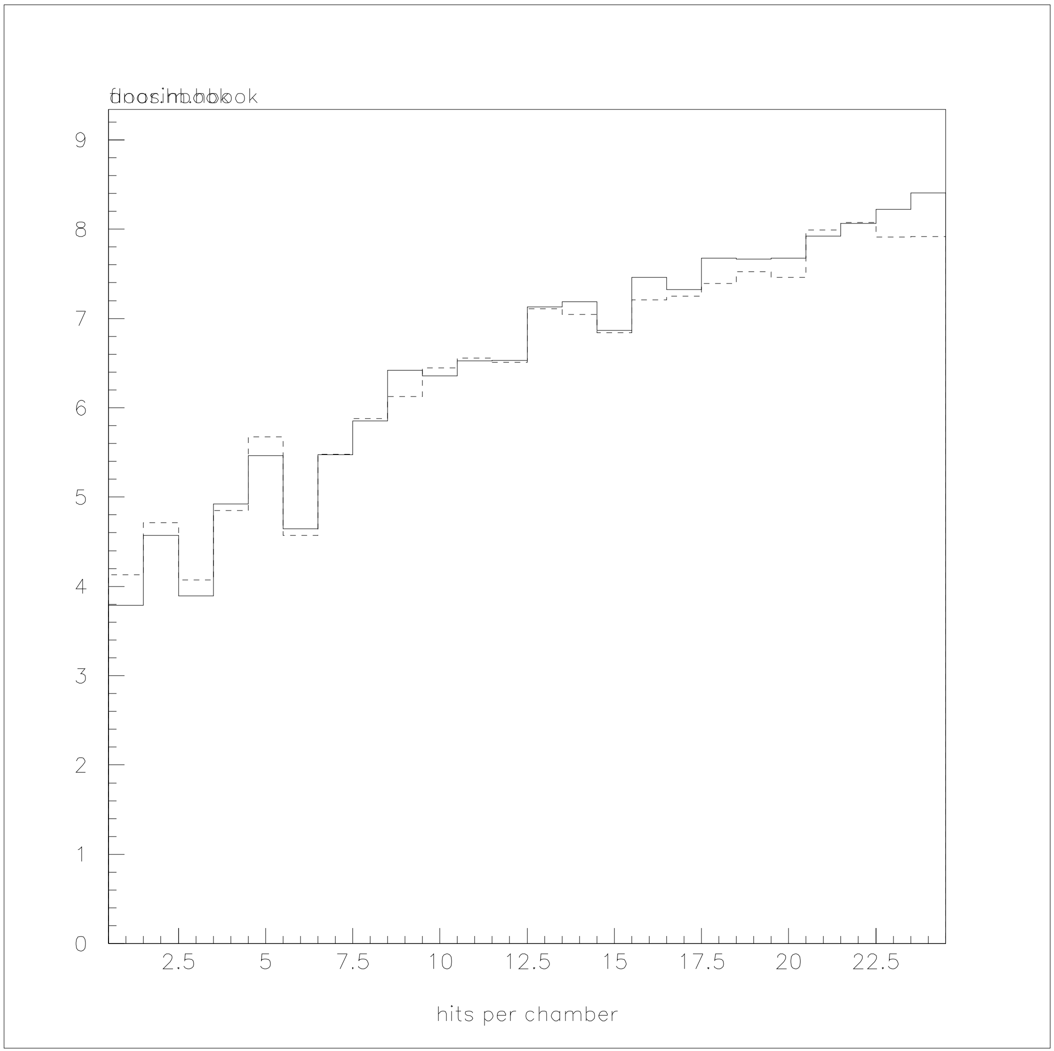

Figure 3.10: Mean number of wire hits in each chamber (solid) and with the chamber frames removed (dashed).

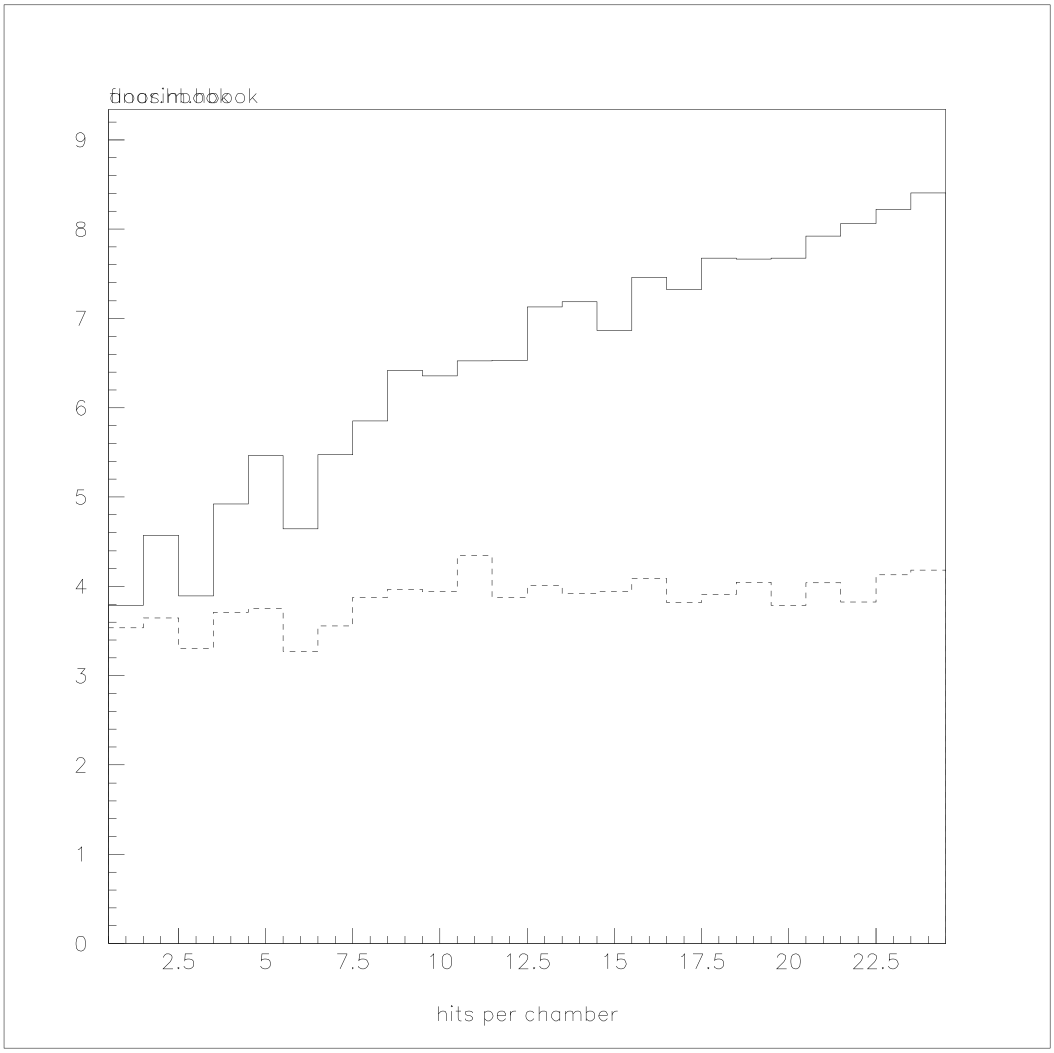

Figure 3.11: Mean number of wire hits in each chamber (solid) and with the beampipe, abort pipe, and chamber frames removed (dashed).

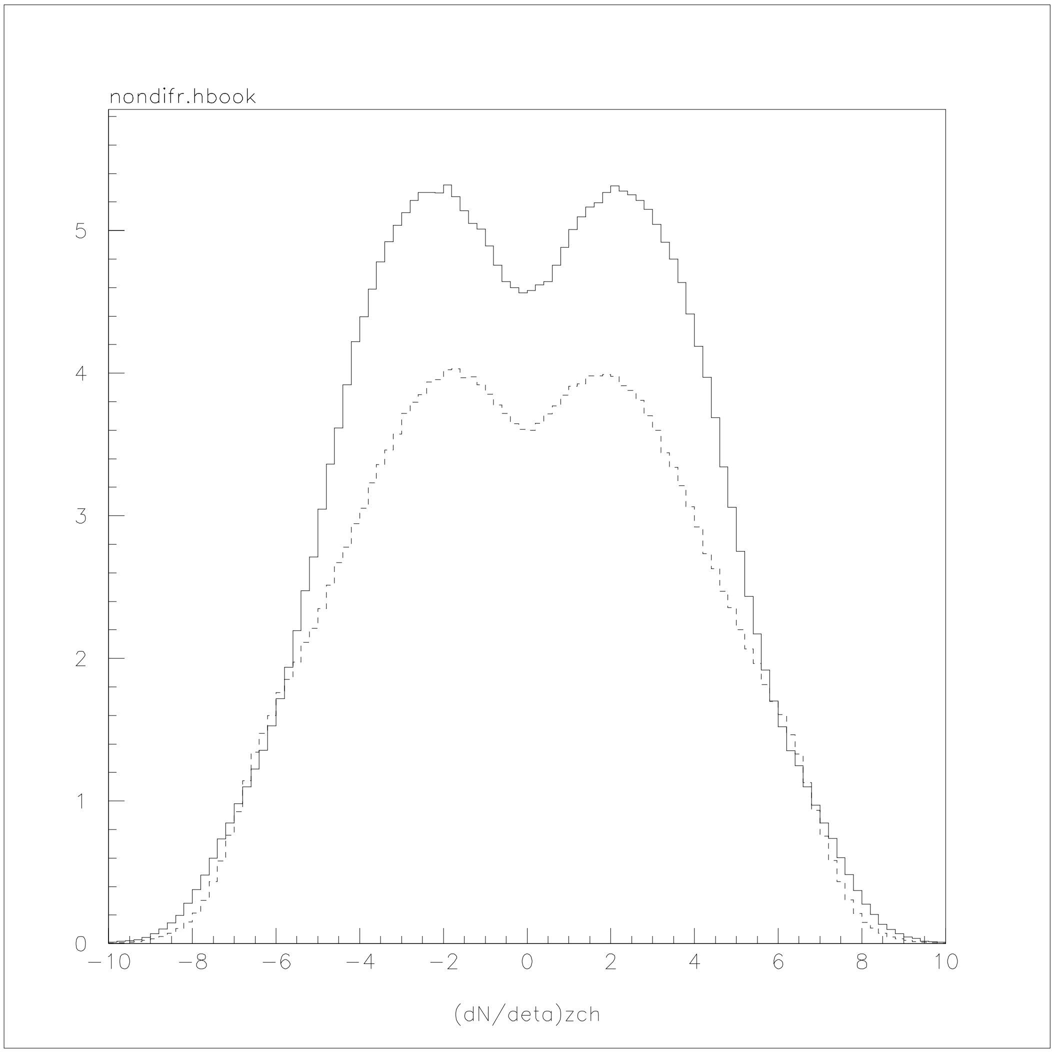

Figure 3.12: Charged-particle multiplicity $dN_{ch}/d\eta$ for non-diffractive PYTHIA (solid) and HERWIG (dashed).

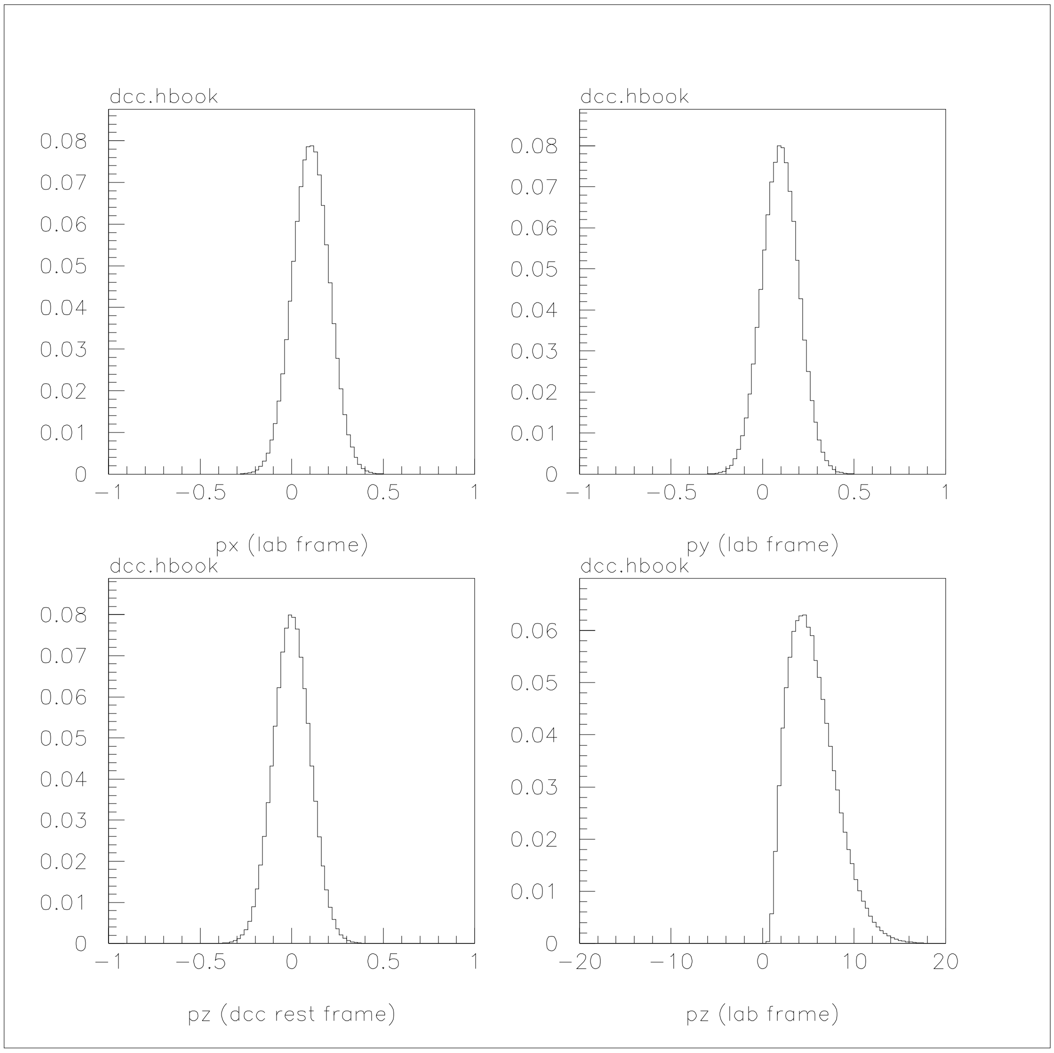

Figure 3.13: Momentum (GeV) of DCC pions: p_x and p_y in lab frame, p_z in DCC rest frame, and p_z in lab frame.

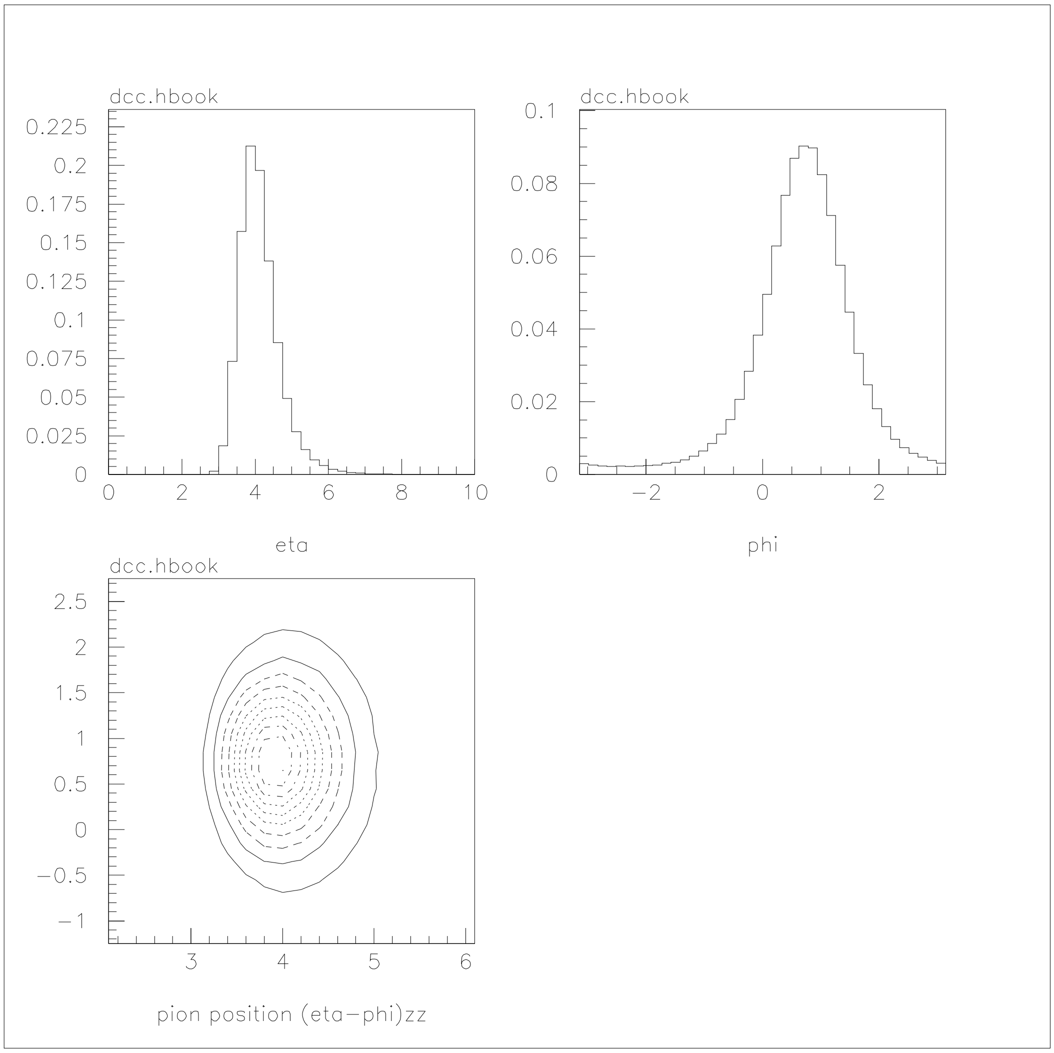

Figure 3.14: Location of the DCC pions in lego space.

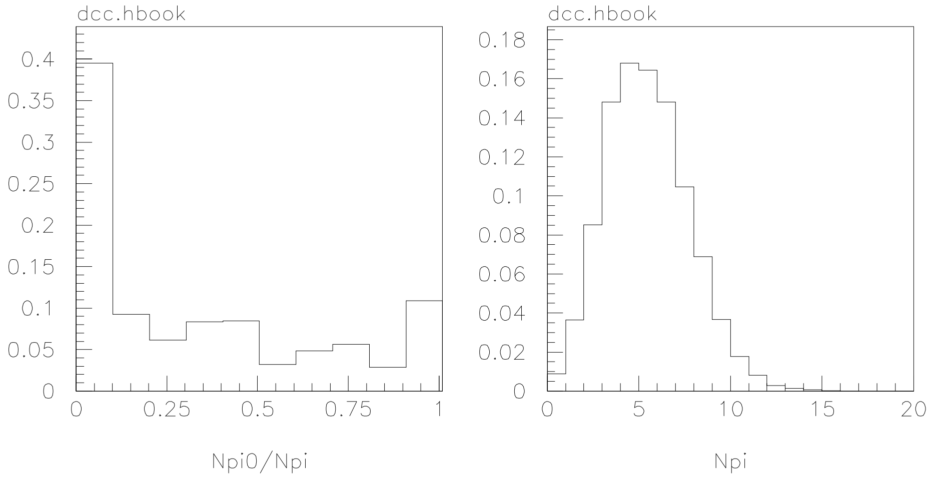

Figure 3.15: Distribution of fraction of DCC pions which are neutral (N_{π^0}/N_π) and total number of DCC pions (N_π).

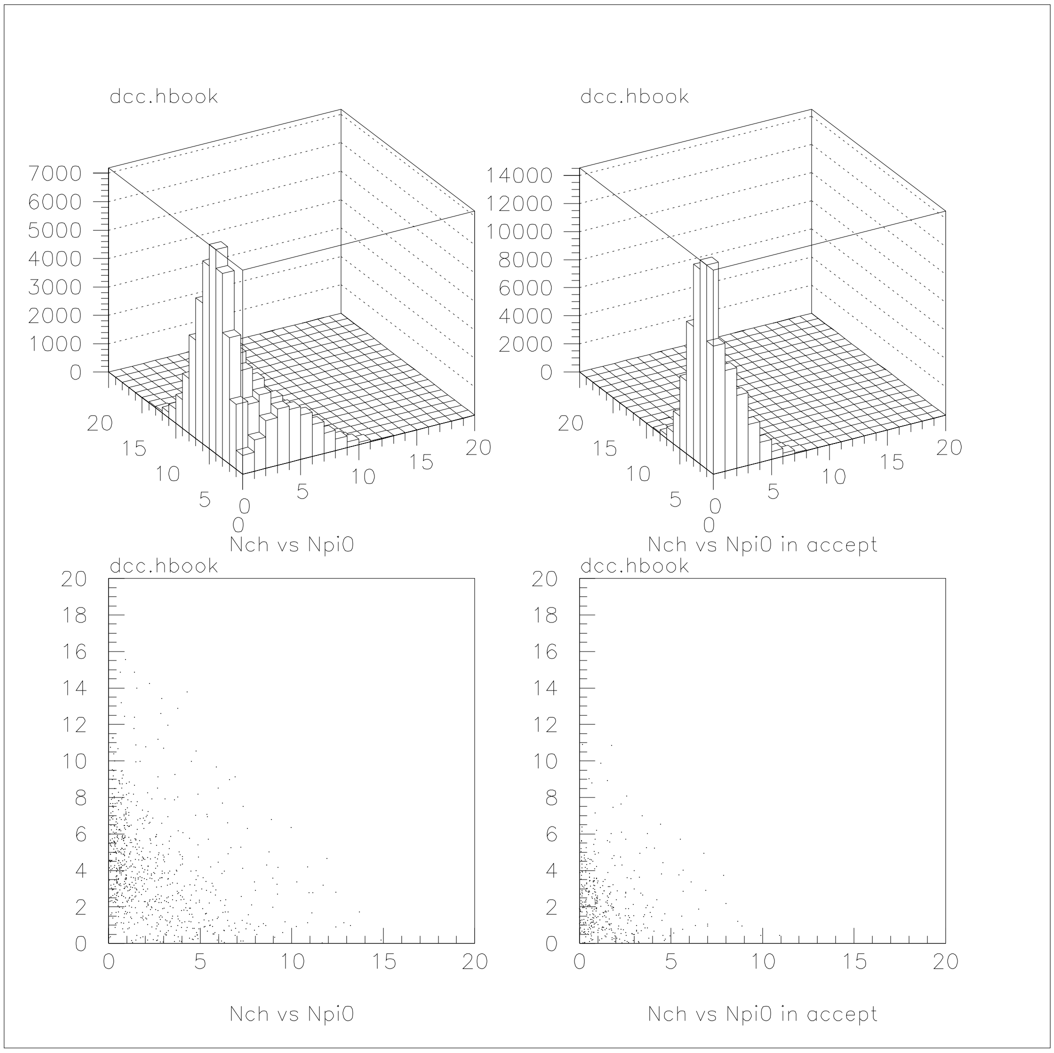

Figure 3.16: Number of charged vs number of neutral DCC pions: total number produced, and the number which enter the MiniMax acceptance.

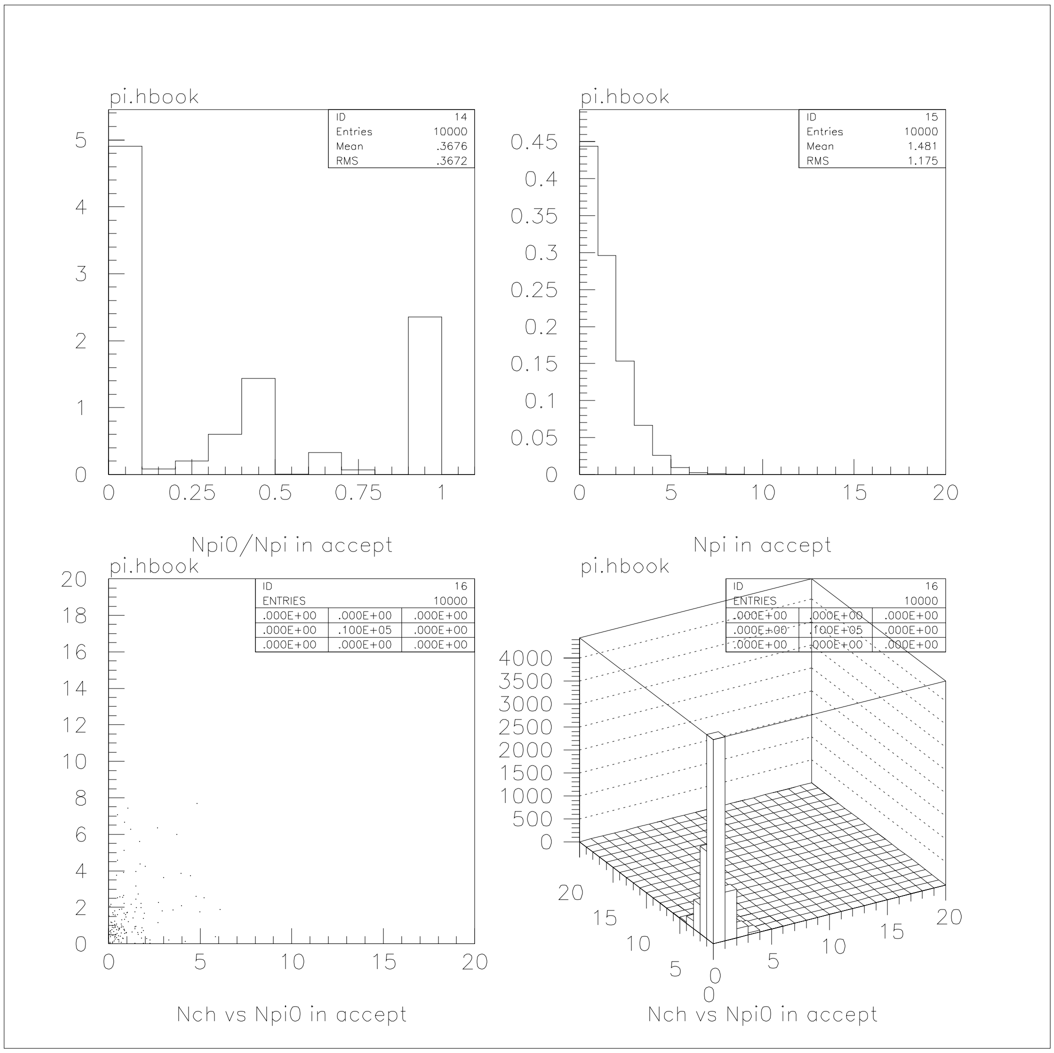

Figure 3.17: Number distributions of pions produced generically (by PYTHIA).

subprocess	cross section (mb)	number of events	GEANT trigger 1 X_0	GEANT trigger fraction	GEANT trigger 0 X_0	GEANT trigger fraction
All included subprocesses	72.98	300000	155709	0.5190	152069	0.5069
f + f' → f + f' (QCD)	2.217	9012	7494	0.8316	7289	0.8088
f + f → f' + f '	0.03198	130	98	0.7538	88	0.6769
f + f → g + g	0.03813	155	122	0.7871	121	0.7806
f + g → f + g	14.67	59642	52456	0.8795	51412	0.8620
g + g → f + f	0.4667	1897	1719	0.9062	1692	0.8919
g + g → g + g	21.42	87072	79857	0.9171	78618	0.9029
Elastic scattering	14.75	60825	0	0.0000	0	0.0000
Single diffractive (XB)	6.194	25525	4057	0.1589	3815	0.1495
Single diffractive (AX)	6.194	25367	2706	0.1067	2452	0.0967
Double diffractive	6.839	28271	5920	0.2094	5336	0.1887
Low-pT scattering	0.1508	2104	1280	0.6084	1246	0.5922

Table 3.1: PYTHIA cross sections and GEANT trigger rates

scint cut/(4 MeV)	pls hgt cut/(0.4 keV)										
	0.00	0.10	0.20	0.30	0.40	0.50	0.60	0.70	0.80	0.90	1.00
0.0	65.24	63.58	62.11	60.82	59.50	58.39	57.45	56.58	55.79	55.16	54.46
0.2	65.24	63.58	62.11	60.82	59.50	58.39	57.45	56.58	55.79	55.16	54.46
0.4	65.24	63.58	62.11	60.82	59.50	58.39	57.45	56.58	55.79	55.16	54.46
0.6	65.24	63.58	62.11	60.82	59.50	58.39	57.45	56.58	55.79	55.16	54.46
0.8	65.24	63.58	62.11	60.82	59.50	58.39	57.45	56.58	55.79	55.16	54.46
1.0	65.24	63.58	62.11	60.82	59.50	58.39	57.45	56.58	55.79	55.16	54.46
1.2	71.32	69.50	67.88	66.47	65.00	63.78	62.74	61.77	60.91	60.21	59.45
1.4	75.45	73.53	71.81	70.31	68.77	67.47	66.36	65.33	64.42	63.68	62.87
1.6	77.16	75.21	73.46	71.93	70.36	69.04	67.92	66.87	65.94	65.19	64.36
1.8	78.35	76.39	74.61	73.05	71.47	70.13	68.99	67.93	66.99	66.22	65.39
2.0	79.37	77.39	75.58	74.00	72.40	71.04	69.88	68.82	67.86	67.08	66.24

Table 3.2: NHITS of "Michgan chambers" in GEANT (threshold = 20) for varying pulse-height and scintillator cuts.